



## Alkyl decorated metal-organic frameworks for selective trapping of ethane from ethylene above ambient pressures

Journal:	<i>Dalton Transactions</i>
Manuscript ID	DT-ART-05-2021-001477.R1
Article Type:	Paper
Date Submitted by the Author:	18-Jun-2021
Complete List of Authors:	Schneemann, Andreas; Technische Universität Dresden, Lehrstuhl für Anorganische Chemie I Jing, Yuan; Hokkaido University Evans, Jack; Chimie ParisTech, Toyao, Takashi; Hokkaido university, Institute for Catalysis Hijikata, Yuh; Hokkaido University, Institute for Chemical Reaction Design and Discovery Kamiya, Yuichi; Hokkaido University, Graduate School of Environmental Earth Science Shimizu, Ken-ichi; Hokkaido University, Catalysis Research Center Burtch, Nicholas; Sandia National Laboratories California, Noro, Shin-ichiro; Hokkaido University, Faculty of Environmental Earth Science

## ARTICLE

## Alkyl decorated metal-organic frameworks for selective trapping of ethane from ethylene above ambient pressures

Andreas Schneemann,<sup>\*a†</sup> Juan Ying,<sup>b</sup> Jack D. Evans,<sup>c</sup> Takashi Toyao,<sup>b,d</sup> Yuh Hijikata,<sup>e</sup> Yuichi Kamiya,<sup>f</sup> Ken-ichi Shimizu,<sup>b,d</sup> Nicholas C. Burtch,<sup>a</sup> and Shin-ichiro Noro<sup>\*f</sup>

Received 00th January 20xx,  
Accepted 00th January 20xx

DOI: 10.1039/x0xx00000x

The trapping of paraffins is beneficial compared to selective olefin adsorption for adsorptive olefin purification from a process engineering point of view. Here we demonstrate the use of a series of  $Zn_2(X\text{-}bdc)_2(\text{dabco})$  (where  $X\text{-}bdc^{2-}$  is  $bdc^{2-}$  = 1,4-benzenedicarboxylate with substituting groups X,  $\text{DM-}bdc^{2-}$  = 2,5-dimethyl-1,4-benzenedicarboxylate or  $\text{TM-}bdc^{2-}$  = 2,3,5,6-tetramethyl-1,4-benzenedicarboxylate and  $\text{dabco}$  = diazabicyclo[2.2.2]octane) metal-organic frameworks (MOFs) for the adsorptive removal of ethane from ethylene streams. The best performing material from this series is  $Zn_2(\text{TM-}bdc)_2(\text{dabco})$  (DMOF-TM), which shows a high ethane uptake of  $5.31 \text{ mmol g}^{-1}$  at 110 kPa, with a good IAST selectivity of 1.88 towards ethane over ethylene. Through breakthrough measurements a high productivity of  $13.1 \text{ L/kg}$  per breakthrough is revealed with good reproducibility over five consecutive cycles. Molecular simulations show that the methyl groups of DMOF-TM are forming a van der Waals trap with the methylene groups from  $\text{dabco}$ , snugly fitting the ethane. Further, rarely used high pressure coadsorption measurements, in pressure regimes that most scientific studies on hydrocarbon separation on MOFs ignore, reveal an increase in ethane capacity and selectivity for binary mixtures with increased pressures. The coadsorption measurements reveal good selectivity of 1.96 at 1000 kPa, which is verified also through IAST calculations up to 3000 kPa. This study overall showcases the opportunities that pore engineering by alkyl group incorporation and pressure increase offer to improve hydrocarbon separation in reticular materials.

### Introduction

Purification and separation processes take up a major part of capital and operating costs in the chemical industry.<sup>1–2</sup> For instance, the separation of light hydrocarbons necessary for the production of polymers is achieved through energy and cost intensive cryo distillation processes. One viable alternative is the use of adsorbent beds filled with microporous materials in temperature and pressure-swing adsorption.<sup>3–4</sup> A class of porous materials that over recent years showed a lot of potential towards separation processes are metal-organic frameworks (MOFs).<sup>5–8</sup> MOFs are constructed by the bridging of inorganic metal containing secondary building units with organic ligands. A nearly infinite amount of combinations

between building blocks is possible, leading to a rich variety of tailorable materials that feature ultrahigh surface areas and tailorable pore spaces.<sup>9–17</sup> Light hydrocarbon separation in MOFs is usually achieved through size-shape exclusion<sup>18–24</sup> or through the presence of interaction sites on the linker<sup>25–27</sup> or the metal-cluster.<sup>28–31</sup> This usually leads to a preferred adsorption of olefins over paraffins, because of the smaller kinetic diameter of the olefin and the stronger interactions between the unsaturated molecule and an open metal site, achieving astonishing adsorption selectivities. Equilibrium based adsorptive separation processes are favored at the industrial scale.<sup>32</sup> However, from an engineering viewpoint, the selective adsorption of the more valuable product, the olefin, is undesired. This would necessitate the inclusion of an additional step to obtain the olefin, requiring a more complex procedure, for instance a two step temperature swing<sup>33</sup> or a displacement desorption process.<sup>34</sup> Adsorbents which selectively scavenge off the paraffin from the gas mixture would facilitate the industrial scale separation of olefin/paraffin mixtures, for example ethane and ethylene. Recently, several strategies have been developed that enabled the selective capture of ethane from ethylene. For instance, the group of Chen showed how the installation of peroxo-sites within  $\text{Fe}_2(\text{dobdc})$  triggered the selective adsorption of ethane over ethylene. Generally speaking, the presence of nonpolar sites and pore surfaces can promote sorption selectivity towards the paraffin.<sup>35–42</sup> Research on aluminophosphates showed, that the installation of methyl groups that line the pore space, induces selective adsorption of

<sup>a</sup> Sandia National Laboratories, 7011 East Avenue, Livermore, CA 94550, United States. E-mail: [Andreas.Schneemann@tu-dresden.de](mailto:Andreas.Schneemann@tu-dresden.de)

<sup>b</sup> Institute for Catalysis, Hokkaido University, Sapporo 001-0020, Japan.

<sup>c</sup> Lehrstuhl für Anorganische Chemie, Technische Universität Dresden, Bergstr. 66, 01069 Dresden, Germany

<sup>d</sup> Elements Strategy Initiative for Catalysis and Batteries, Kyoto University, Katsura, Kyoto 615-8520, Japan.

<sup>e</sup> Institute for Chemical Reaction Design and Discovery (WPI-ICReDD), Hokkaido University, Sapporo 001-0021, Japan

<sup>f</sup> Faculty of Environmental Earth Science, Hokkaido University, Sapporo 060-0810, Japan. E-mail: [noro@ees.hokudai.ac.jp](mailto:noro@ees.hokudai.ac.jp)

<sup>†</sup> Current Address: Lehrstuhl für Anorganische Chemie, Technische Universität Dresden, Bergstr. 66, 01069 Dresden, Germany

Electronic Supplementary Information (ESI) available, including detailed synthetic procedures, PXRD, IR spectroscopy, TGA, SEM,  $\text{N}_2$  physisorption isotherms, isotherm fits and tabulated coadsorption data. See DOI: 10.1039/x0xx00000x

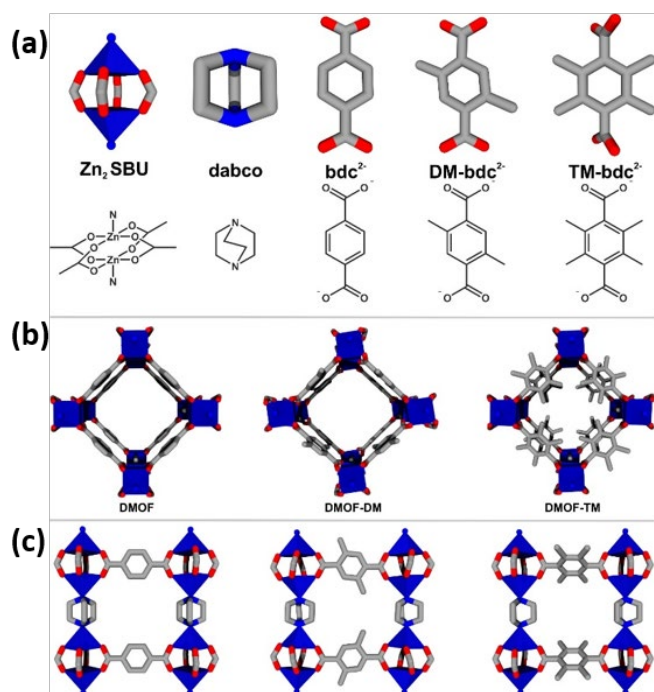


**Figure 1:** (a) Depiction of the building blocks used for the construction of DMOF, DMOF-DM and DMOF-TM. (b) View along the c-axis of the three materials. (c) View along the a/b axis of the materials. Carbon, oxygen and nitrogen atoms have been depicted in grey, red and blue respectively. Blue polyhedrons represent coordination environment around Zn. Hydrogen atoms have been omitted for clarity.

ethane over ethylene.<sup>43-44</sup> Building up on this approach, we showcase the possibility of using an isorecticular series of pillared-layered MOF featuring diazabicyclo[2.2.2]octane (dabco) pillars and 1,4-benzenedicarboxylate (bdc<sup>2-</sup>) ligands with varying amounts of methyl groups attached to the linker backbone. Apart from the prototypical Zn<sub>2</sub>(bdc)<sub>2</sub>(dabco) (**DMOF**) framework, two MOFs using H<sub>2</sub>R-bdc ligands (with H<sub>2</sub>X-bdc = H<sub>2</sub>DM-bdc = 2,5-dimethyl-1,4-benzenedicarboxylic acid and H<sub>2</sub>TM-bdc = 2,3,5,6-tetramethyl-1,4-benzenedicarboxylic acid), namely Zn<sub>2</sub>(DM-bdc)<sub>2</sub>(dabco) (**DMOF-DM**) and Zn<sub>2</sub>(TM-bdc)<sub>2</sub>(dabco) (**DMOF-TM**) were prepared (Figure 1). Materials **DMOF-DM** and **DMOF-TM** feature two and four methyl groups on the linker backbone, respectively. In these materials, Zn<sub>2</sub> paddlewheels are bridged via benzenedicarboxylate linkers, establishing Zn<sub>2</sub>(R-bdc)<sub>2</sub> 2D grids. These grids are stacked into the third dimension by dabco pillars, forming a 3D structure. On the one hand attaching methyl groups reduces the pore space and on the other hand decreases the polarity of the pore. For instance, the most polar adsorption sites<sup>45</sup> in paddle-wheel based pillared-layered MOFs located at the O-M-O pockets are partially blocked through the methyl groups. Previous studies on these systems, highlight the potential of methyl groups to alter the moisture resistance,<sup>46-48</sup> framework dynamics,<sup>49</sup> SO<sub>2</sub> capture,<sup>50</sup> as well as thermal properties<sup>51-52</sup> of these frameworks. Here these frameworks were analysed towards their feasibility as adsorbents for selective ethane adsorption using low and high pressure adsorption isotherms, coadsorption measurements as well as breakthrough experiments, supported through molecular simulations. Particularly, we want to highlight the adsorption properties of

the materials above ambient pressures. Recently, Pires and coworkers have raised awareness that while there is a lot of well performing ethane selective MOF materials, their use might be hampered by the fact that they reach their full ethane uptake at too low pressures, making them unfeasible for pressure swing adsorption application which operate between 100 and 1000 kPa.<sup>53</sup> Hence, we present high pressure adsorption isotherms up to 3000 kPa as well as coadsorption experiments up to 1800 kPa to verify our materials performance at these more suitable pressures. Furthermore, a recent study highlighted the necessity of reliable coadsorption data in the literature<sup>54</sup> and we provide data sets that will be helpful to the simulations and machine learning community in the supporting information.

## Experimental Section

All chemicals were obtained from commercial vendors without further purification unless otherwise stated. All gases used for adsorption or breakthrough experiments had purities of 99.9% or higher.

### Syntheses

1 mmol H<sub>2</sub>X-bdc (for weights see supporting information), Zn(NO<sub>3</sub>)<sub>2</sub>·6H<sub>2</sub>O (1mmol, 298 mg) and dabco (0.7 mmol, 78 mg) were put in a scintillation vial and 20 mL of dimethylformamide (DMF) were added. The mixture was sonicated for 10 minutes and afterwards placed in an isothermal oven at 120 °C for 24h. Afterwards, the reaction mixture was cooled to room temperature and the mixture was transferred into centrifugation tubes. After centrifugation (8700 rpm, 3 min) the DMF was removed and replaced with fresh DMF. The DMF was replaced twice with fresh DMF and three times with dichloromethane. Afterwards the samples were dried in vacuo (120 °C, overnight) and transferred into a glovebox until further manipulation. For yields see supporting information.

### Analytical Methods

Powder X-ray diffraction patterns were acquired on a Rigaku Smartlab diffractometer using Cu-Kα radiation operated at 44 kV and 40 mA. The material was placed on a glass slide and put on the Z-Phi stage and the scans were performed in 2Theta mode. Infrared Spectra were measured on an Agilent Technologies Cary-630 instrument equipped with an ATR unit located in a glovebox. Prior to each measurement, a background spectrum was collected and subtracted. Field-emission scanning electron microscopy images were captured using a Hitachi S-4800 at an acceleration voltage of 1 kV. Thermogravimetric Analysis (TGA) Measurements were conducted on a RIGAKU Thermo plus EVO2 TG-DTA8122. The samples were heated from 30 to 500 °C with a heating rate of 10 °C min<sup>-1</sup> and under a constant N<sub>2</sub> flow of 100 mL min<sup>-1</sup>. The Nitrogen physisorption isotherms were obtained using a Micromeritics ASAP 2020 porosimeter at 77K using a N<sub>2</sub> bath for cooling using 50-100 mg of sample. The samples were degassed on the activation port of the instrument in vacuo overnight at elevated temperatures (120 °C). Low pressure ethane and

ethylene adsorption isotherms (0-100 kPa) were measured at 288, 298 and 308 K, using a Belsorp Mini adsorption instrument from Microtrac Bel. The samples were filled into pre-weighted sample tubes. Prior to measurements the samples were evacuated and heated to 120 °C on a Belprep (Microtrac Bel) sample preparation station, for the first measurement overnight and for every subsequent measurement for at least three hours. The measurement temperature was controlled using a constant temperature water circulator. High pressure adsorption measurements up to 3000 kPa were conducted using a Belsorp VC from Microtrac Bel. The sample holder was filled with 0.5-1 g of sample and installed in the isothermal box of the measurement instrument. The sample was evacuated prior to each measurement. Co-adsorption measurements were as well performed on a Belsorp VC. For the measurements, the gases were mixed inside the manifold of the instrument and afterwards the sample was exposed to the gas mixture. After the equilibration requirements were fulfilled, an aliquot of the gas atmosphere above the adsorbent was sampled and injected into a Agilent 490 Micro gas chromatographic system equipped with a thermal conductivity detector. Breakthrough experiments for ethane/ethylene mixtures with 1:1 ratio were carried out at a flow rate of 6 mL/min at 298 K under ambient pressure. The MOF powder (920 mg) was placed into a  $\phi 4 \times 350$  mm glass cell. Prior to measurements, the samples were subjected to pretreatment (120 °C, 1 h) under a flow of He (50 mL/min). The flow rates of all gas mixtures were regulated by mass flow controllers, and the effluent gas stream was monitored by a TCD GC (990 Micro GC; Agilent Technologies Inc.) equipped with a PorapLOT Q column. Cycling experiments were performed in a manner similar to that described above. Following the breakthrough experiment, the sample was heated at 120 °C for 1 h under a flow of He (50 mL/min), and then reused for an ensuing experiment.

### Processing of Adsorption Isotherms

Low pressure adsorption isotherms were fit using the dual site Langmuir Freundlich equation:

$$n_{ads} = \frac{n_{max,1} \cdot k_1 \cdot p^{v_1}}{1 + k_1 \cdot p^{v_1}} + \frac{n_{max,2} \cdot k_2 \cdot p^{v_2}}{1 + k_2 \cdot p^{v_2}}$$

In this equation  $n_{max,i}$  is the adsorbed amount for each adsorption site at saturation,  $k_i$  is the Langmuir coefficient and  $v_i$  is the dimensionless Freundlich parameter. The determined fitting parameters for the low pressure (0-100 kPa at 288, 298 and 308K) adsorption isotherms are tabulated in the supporting information. The fitting parameters of the isotherms were used to determine the respective heats of adsorption ( $Q_{st}$ ) using the Clausius-Clapeyron<sup>55</sup> Equation:

$$Q_{st} = RT^2 \left( \frac{\partial \ln p}{\partial T} \right)_n$$

Furthermore, the fits of the single component isotherms measured at 298 K (low pressure and high pressure) were used

to calculate sorption selectivities based on the ideal adsorbed solution theory<sup>56</sup> (IAST):

$$S_{ads} = \frac{q_1/q_2}{p_1/p_2}$$

here  $q_i$  represents the molar fraction of the gas in the gas phase and  $p_i$  the molar fraction of the gas in the adsorbate phase.

For the high pressure adsorption data, the obtained excess adsorptions ( $n_{exc}$ ) were transformed to total adsorption ( $n_{tot}$ ):

$$n_{tot} = n_{exc} + \rho_g \cdot V_g$$

whereas  $\rho_g$  is the pressure and temperature dependent density of the adsorbate derived from their respective equation of state and  $V_g$  is the void volume of the adsorbent derived from their single crystal structure.

In order to circumvent issues associated with the extraction of adsorption data for data mining<sup>57</sup> and machine learning purposes, we deposited all obtained C2 adsorption isotherms online using the recently established adsorption isotherm file format.<sup>58</sup> Isotherm data is free of charge accessible in the electronic supplementary information.

### Molecular simulation

Molecular representations of **DMOF**, **DMOF-DM** and **DMOF-TM** pore structures were generated from the unit cells of their respective crystal structures. The resulting molecular pore structures contain eight paddlewheel units connected by eight carboxylate ligands and four dabco molecules to produce a cube. The paddlewheel units facing the outside of this pore are capped by formate and ammonia units.

The pore structure interaction with ethane and ethylene were subsequently investigated by a combination of classical potentials and semiempirical tight-binding approaches, namely GFN-FF and GFN2-xTB.<sup>59-60</sup> Low energy binding conformations of one gas molecule within the pore structure were identified using extensive metadynamic sampling as implemented in the Conformer-Rotamer Ensemble Sampling Tool (CREST).<sup>61</sup> An ellipsoid potential was applied to counteract the bias potentials during the simulations which could produce complete dissociation of the gas from the molecular pore structure. Initially binding confirmations within a 125.52 kJ mol<sup>-1</sup> window were screened using the GFN-FF classical potential and 10 unique 10 ps metadynamics trajectories followed by geometry optimisations. The resulting binding confirmations were then further screened by optimisation with the accurate and efficient GFN2-xTB method. The relative energy of the identified binding modes were calculated at the GFN2-xTB level of theory. Representative input files for molecular simulations are available online in the data repository <https://github.com/jackevansadl/supp-data>.

### Results and Discussion

The materials were synthesized from Zn(NO<sub>3</sub>)<sub>2</sub>·6H<sub>2</sub>O, dabco and the respective dicarboxylic acid, using solvothermal synthesis in DMF. The materials were obtained as white microcrystalline

powders and activated after solvent exchange with dichloromethane via evacuation at elevated temperatures. Phase purity was confirmed using powder X-ray diffraction and proper activation and absence of the synthesis solvent through IR-spectroscopy, N<sub>2</sub> adsorption and Thermogravimetric Analysis (See ESI S1-S5). The BET surface area decreases with increasing amount of methyl groups inside the pore space, from 1779.9 m<sup>2</sup> g<sup>-1</sup> to 1133.8 m<sup>2</sup> g<sup>-1</sup> and to 962.5 m<sup>2</sup> g<sup>-1</sup> for **DMOF**, **DMOF-DM** and **DMOF-TM** respectively and are matching with previous reports of these materials.<sup>48, 62-63</sup> All samples were obtained with polydisperse crystal size distribution in the range from submicron size to 50 μm (see SEM micrographs in ESI S6), unlike in kinetic adsorption<sup>64-66</sup> or dynamic MOF systems<sup>67-69</sup> which are studied elsewhere, this broad size distribution is neglectable for the scope of this study reporting hydrocarbon separation at thermodynamic equilibrium.

### Low Pressure Adsorption Studies

The ethane and ethylene adsorption isotherms recorded at 298 K from 0-110 kPa are shown in Figure 2. For all three materials a distinct adsorption selectivity towards C<sub>2</sub>H<sub>6</sub> is visible. At 110 kPa C<sub>2</sub>H<sub>6</sub> uptakes of 2.79, 4.03 and 5.31 mmol g<sup>-1</sup> were observed for material **DMOF**, **DMOF-DM** and **DMOF-TM**, respectively. The ethylene uptakes on the other hand are lower at 110 kPa and amount to 2.08, 3.11 and 4.99 mmol g<sup>-1</sup> for the three materials. The ethane uptake is slightly lower than for the related compound Ni<sub>2</sub>(TM-bdc)<sub>2</sub>(dabco) (5.45 mmol at 100 kPa).<sup>70</sup> It is also visible from the isotherms that decreasing the pore size by adding methyl groups, leads to a steeper slope in the isotherms, we attribute this to the better fit of the gases into the confined pore space, which enhances uptake at low pressures. In the cases of **DMOF-TM** it appears that saturation is nearly reached at 110 kPa, while for **DMOF** and **DMOF-DM** the isotherms did not reach a plateau yet. Interestingly, at around 50 kPa a small step can be observed in the C<sub>2</sub>H<sub>6</sub> adsorption isotherm of **DMOF-DM** (See supporting information

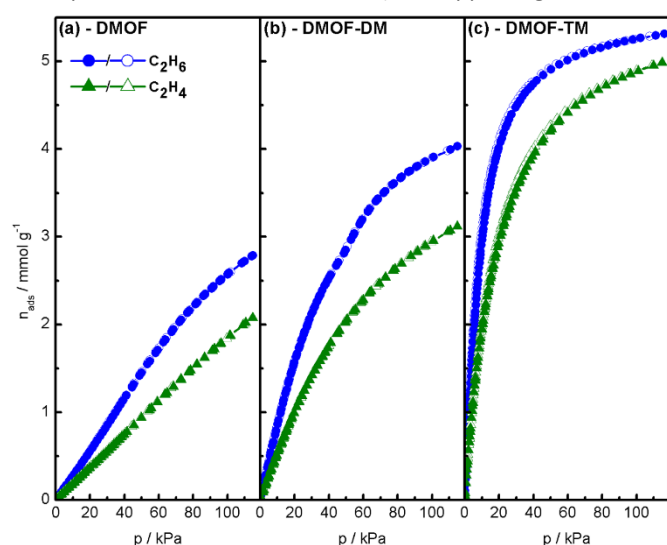


**Figure 2:** Ethane (blue circles) and ethylene (green triangles) sorption isotherms for **DMOF** (a), **DMOF-DM** (b) and **DMOF-TM** (c) measured at 298 K. Filled and empty symbols represent adsorption and desorption branches, respectively.

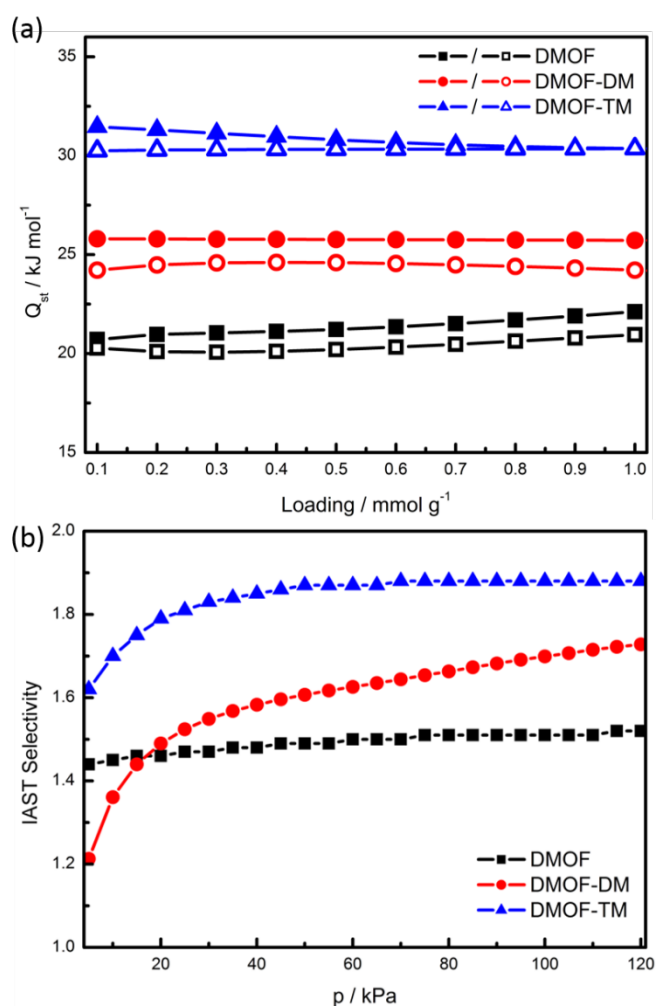


**Figure 3:** (a) Isothermic heats of adsorption of **DMOF** (black squares), **DMOF-DM** (red circles) and **DMOF-TM** (blue triangles) for ethane (filled symbols) and ethylene (closed symbols). (b) IAST selectivities towards ethane over ethylene for equimolar mixtures of **DMOF** (black squares), **DMOF-DM** (red circles) and **DMOF-TM** (blue triangles).

for logarithmic plots). We believe that this is not an artefact, as it also is observed in measurements at 288 K and 308 K and also when a different batch of the material was measured on another instrument. This is attributed to small structural changes that have been observed for this class of material, i.e. during the adsorption of different solvent<sup>62</sup> or vapour guests,<sup>71</sup> in some extreme cases a so called “breathing” effect can be observed for Zn-based pillared layered MOFs.<sup>72-74</sup> It is somewhat puzzling why this is not observed for the case of **DMOF-TM** as well, potentially this is due to the presence of four methyl groups per linker which restrict the cooperative movement of the framework.

Adsorption isotherms at 288 and 308 K were also recorded, in order to determine the  $Q_{st}$  through the Clausius-Clapeyron equation (Figure 3a). For this, the isotherms were fit using dual site Langmuir Freundlich isotherms (for isotherm fits and tabulated coefficients see ESI Fig S6-S13) At a loading of 0.1 mmol g<sup>-1</sup> the calculated  $Q_{st}$  of C<sub>2</sub>H<sub>6</sub> and C<sub>2</sub>H<sub>4</sub> are 20.7 and 20.3 kJ mol<sup>-1</sup>, 25.8 and 24.2 kJ mol<sup>-1</sup> and 31.5 and 30.2 kJ mol<sup>-1</sup>, for **DMOF**, **DMOF-DM** and **DMOF-TM** respectively. These values are in contrast to the results of Ma and coworkers on related Ni<sub>2</sub>(TM-bdc)<sub>2</sub>(dabco),<sup>70</sup> which obtained substantially higher  $Q_{st}$

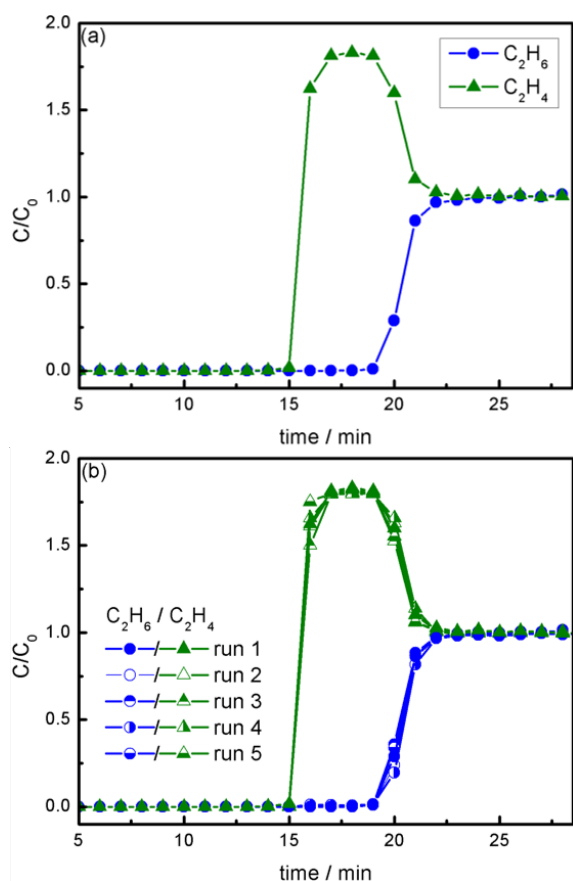


**Figure 4:** (a) Ethylene (green triangles) and ethane (blue circles) breakthrough curves for **DMOF-TM** measured at 298 K. (b) Depiction of five consecutive runs over the same material using an equimolar  $C_2H_6/C_2H_4$  mixture. Lines are a guide to the eye only.

towards  $C_2H_6$  of around  $39 \text{ kJ mol}^{-1}$  and attributed the  $C_2H_6$  adsorption selectivity to strong host-guest interactions. However, good selectivity paired with relatively low heats of adsorption are considered advantageous as regeneration of the adsorbent bed needs less energy input. This would make the Zn based framework more suitable for separations compared to the Ni analogue. The results obtained from **DMOF-DM** need to be taken with some care, since the step like feature in the  $C_2H_6$  adsorption isotherm made it difficult to fit a reasonable equation precisely and it may be prone to error.

Furthermore IAST selectivities were calculated from the dual site Langmuir Freundlich Fits of the isotherms at 298 K and the results are shown in Figure 3b. For an equimolar mixture of ethane and ethylene at 100 kPa the IAST values amount to 1.51, 1.70 and 1.88 respectively. These values are in line with results on similar Ni based materials, however only results for a 1:15 ethane to ethylene mixture were presented. Other high performers, i.e. MUF-15 or PCN-250 are in the same selectivity region as **DMOF-TM**, while  $Cu(Qc)_2$  and  $Fe_2(O_2)(dobdc)$  have larger selectivities, but lower overall ethane uptakes. A detailed discussion can be found at the end of this manuscript.

The very promising results derived from the single component adsorption isotherms motivated us to conduct breakthrough measurements on **DMOF-TM** at 100 kPa with an equimolar mixture of  $C_2H_6$  and  $C_2H_4$ . For this, approximately 1 g of material was packed into a column and an ethane/ethylene mixture was

flowed over the material while monitoring the  $C_2H_6$  and  $C_2H_4$  concentration at the outlet. The breakthrough curves are depicted in Figure 4. After flowing the gas mixture for 16 minutes over the **DMOF-TM** bed a response is measured at the outlet. The gas chromatography suggests that it is pure ethylene, while the ethane is retained in the pore space of the **DMOF-TM** bed. The first signal for ethane is observed after 19 minutes. After 22 minutes the ethane and ethylene concentration at the outlet are equivalent to the feed concentration. These measurements are highly reversible, Figure 4b shows 5 consecutive runs of equimolar  $C_2H_6/C_2H_4$  mixtures, all showing identical curves. Through integration of the area under the curve at which the  $C_2H_4$  concentration in the outlet stream is  $>99.95\%$  the ethylene productivity can be calculated, which has been done as described by Qazvini.<sup>37</sup> **DMOF-TM** shows a high productivity value of  $13.1 \text{ L kg}^{-1}$ , which is only slightly lower than the ethylene productivity of other high performance ethane selective MOF. For comparison  $Fe_2(O_2)(dobdc)$ <sup>75</sup> and MUF-15<sup>37</sup> have experimentally determined productivities of 19.3 and  $14 \text{ L kg}^{-1}$  respectively.

#### Computational Determination of Preferential Adsorption Sites

To further examine the observed adsorption selectivities, we employed molecular simulations to identify the favourable adsorption sites for ethane and ethylene in **DMOF**, **DMOF-DM** and **DMOF-TM**. For the material **DMOF**, a similar picture of the favoured adsorption sites as for other pillared layered MOFs is revealed. The most favoured adsorption site for both ethane and ethylene is directly located at the corner of the pore at the O-Zn-O pocket, with potential interactions with the benzene rings and hydrogen bonding to the oxygens (Figure 5a and d). For other pillared layered MOFs, for instance alkyl ether functionalized **DMOF**, this site was also determined to be the best adsorption site for  $CO_2$ .<sup>45</sup> Furthermore, adsorption enthalpies could be derived for the favoured adsorption sites, which amounted to  $-24.6 \text{ kJ mol}^{-1}$  and  $-23.8 \text{ kJ mol}^{-1}$  for ethane and ethylene, respectively (See ESI Figure S19 for adsorption enthalpies for the range of low energy adsorption positions). These values are in a similar range as the  $Q_{st}$  values obtained from the Clausius-Clapeyron equation. For ethane the favoured adsorption sites on **DMOF-DM** are located in a pocket constructed by the methyl groups provided by three individual DM-bdc<sup>2-</sup> linkers and the  $CH_2$  groups from the dabco pillar (Figure 5b). The ethylene sits in a similar pocket in proximity to two  $CH_3$  groups on the DM-bdc<sup>2-</sup> linker, the  $CH_2$  units from the dabco and the oxygen from the  $Zn_2O_8N_2$  metal-cluster. The adsorption enthalpies are considerably higher than for unfunctionalized **DMOF**, amounting to  $-28.4 \text{ kJ mol}^{-1}$  and  $-27.6 \text{ kJ mol}^{-1}$  for ethane and ethylene, respectively, qualitatively matching the results obtained from the  $Q_{st}$  calculations. Interestingly, this simulation approach also allowed the host framework to deform to produce pore rearrangement also observed in other flexible MOFs to accommodate guest molecules more snugly. For instance Wriedt et al. reported the rearrangement of an elastic  $CO_2$  trap during low pressure adsorption of  $CO_2$ .<sup>76</sup> Lastly, for **DMOF-TM**, the material with the highest amount of  $sp^3 CH_2$  and  $CH_3$  groups anchored in the pore

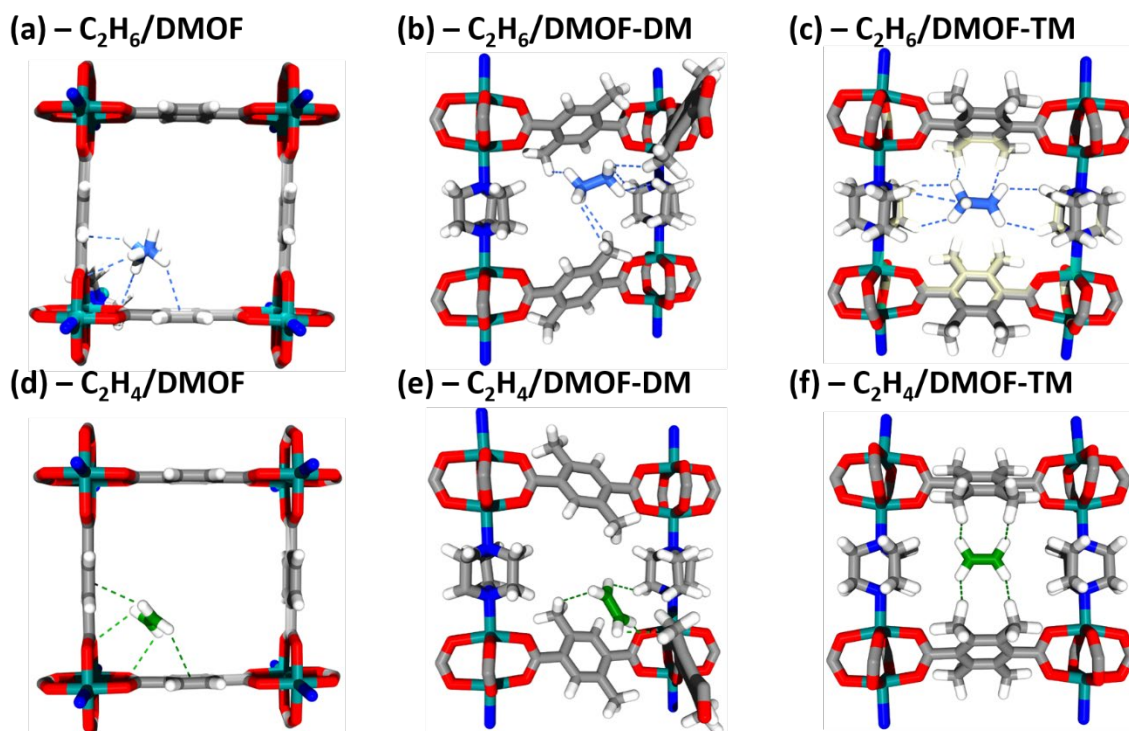


**Figure 5:** Illustration of the energetically favoured adsorption sites for ethane (a-c) and ethylene (d-f) in **DMOF** (a, d), **DMOF-DM** (b, e) and **DMOF-TM** (c, f) derived through DFT calculations. C, H, O, N and Zn are represented in grey, white, red, blue and teal, respectively. Carbon atoms of ethane and ethylene are represented in light blue and green, respectively. Dotted lines between guest molecules and framework represent closest contacts. For the sake of clarity parts of the framework have been omitted from the graphical representation.

space and hence the least polar pore space, the highest adsorption enthalpies were calculated. Surprisingly, the highest adsorption enthalpy was found for ethylene, amounting to  $-30.8 \text{ kJ mol}^{-1}$ , while the adsorption enthalpy for ethane on **DMOF-TM** was calculated to be  $-28.8 \text{ kJ mol}^{-1}$ . The favoured adsorption position for ethane in **DMOF-TM** is located at the pore aperture, interacting with two dabco molecules and with two neighbouring methyl groups on one TM-bdc<sup>2-</sup> linker (Figure 5c). Notably, ethylene is also sitting in the pore entrance build up by two dabco and two TM-bdc<sup>2-</sup> linkers, perfectly fitting in between the opposing TM-bdc<sup>2-</sup>, interacting with four methyl groups. The adsorption enthalpies for **DMOF-TM** do not fully match with the values obtained from the  $Q_{st}$  calculations, however, the calculated enthalpies only reflect a single site,

while the  $Q_{st}$  calculations involve a range of sites occupied during the adsorption process. Furthermore, it needs to be noted that the amount of different high enthalpy adsorption sites is higher for ethane compared to ethylene on **DMOF-TM** as shown in Figure S19. Interestingly, our results nicely confirm earlier suggestions by Kroon and coworkers who highlighted the affinity of methylated aluminophosphates towards paraffins over olefins. It is particularly interesting that the guest molecules are favourably adsorbing in proximity to non-polar interaction sites with mostly van der Waals interactions responsible for the strong adsorption, making the highly methylated frameworks **DMOF-DM** and **DMOF-TM** efficient van der Waals traps for C2 hydrocarbons.

#### High Pressure Adsorption Studies

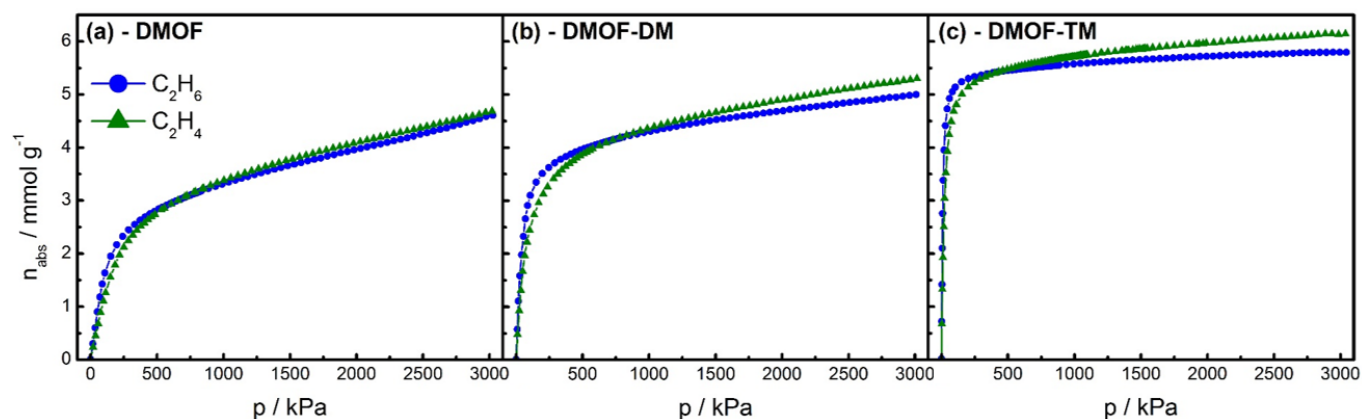


**Figure 6:** Ethane (blue circles) and ethylene (green triangles) adsorption isotherms of **DMOF** (a), **DMOF-DM** (b) and **DMOF-TM** (c) measured at 298 K. Lines connecting the dots are a guide to the eyes only.

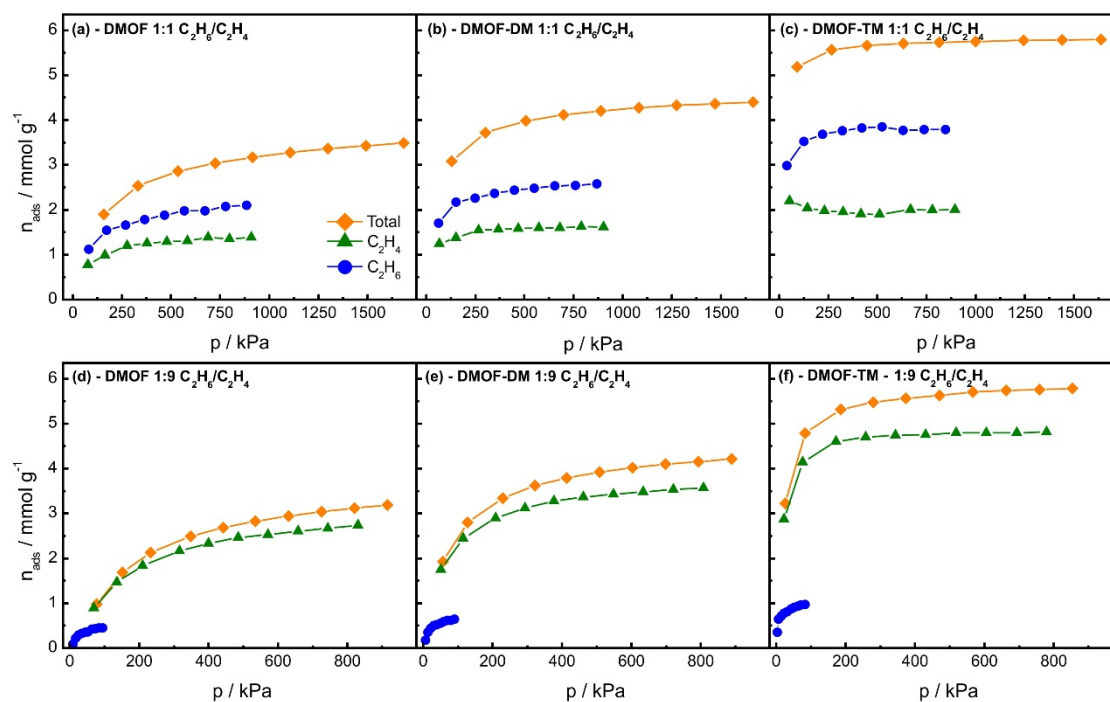


**Figure 7:** Co-adsorption measurements on **DMOF** (a, d), **DMOF-DM** (b, e) and **DMOF-TM** (c, f). At varying total pressures between 100 and 1700 kPa 50:50 (a-c) and 10:90 (d-f) mixtures of  $C_2H_6:C_2H_4$  were dosed onto the samples. Orange diamonds represent total adsorption, green triangles and blue circles represent  $C_2H_4$  and  $C_2H_6$  adsorption respectively.

High Pressure adsorption isotherms were measured at 298 K in a range from 0-3000 kPa for ethylene and ethane. The measured isotherms were transformed from excess adsorption to total adsorption ( $n_{tot}$ ) using the temperature dependent density of the adsorbates derived from the respective equations of state for ethylene<sup>77</sup> and ethane.<sup>78</sup> The data is displayed in Figure 6. In all cases the ethane and ethylene graphs are intersecting, in a way that the ethane uptake is higher at low pressures, while the ethylene uptake is higher at high pressures. The intersection occurs at approximately 660, 730 and 430 kPa for **DMOF**, **DMOF-DM** and **DMOF-TM**, respectively. The total uptakes at 3000 kPa for **DMOF** amount to approximately 4.6 and 4.68 mmol  $g^{-1}$  in the cases of  $C_2H_6$  and  $C_2H_4$ . A slightly higher uptake is recorded for **DMOF-DM** with 5.0 and 5.3 mmol  $g^{-1}$  of ethane and ethylene, respectively. The highest uptakes are observed for **DMOF-TM**, with values of 5.79 mmol  $g^{-1}$  for ethane and 6.14 mmol  $g^{-1}$  for ethylene. Interestingly, the condensation pressures for ethane and ethylene are still considerably higher than 3000 kPa at 298 K. These applied pressures are capturing the range used in pressure swing adsorption application which operate between 100 and 1000 kPa.<sup>53</sup> Giving also potential use for **DMOF** and **DMOF-DM**, however, their selectivities are comparably low, as discussed in the IAST section and the Co-adsorption section. According to this **DMOF** and **DMOF-DM** would have ethane adsorption working capacities of 1.71 and 1.21 mmol in the range of 100-1000 kPa, while the working capacity of **DMOF-TM** only amounts to 0.45 mmol in this pressure regime.

#### High Pressure Co-adsorption Measurements

In order to assess the adsorption selectivity towards ethane and to investigate how the mixture behaves above the intersection of the isotherms, co-adsorption measurements were conducted in the region from 0 to 1000 kPa for a 50:50 and a 10:90

$C_2H_6/C_2H_4$  mixture. Co-adsorption measurements are thus far rarely used for the analysis of MOFs,<sup>79-85</sup> we recently described the use co-adsorption measurements for the analysis of olefin selective MOFs with open metal sites<sup>86</sup> and the response of flexible MOFs to gas mixtures.<sup>26</sup> During these measurements both gases are exposed simultaneously to the sample and after equilibration a portion of the gaseous phase above the adsorbent is sampled via gas chromatography to determine the gas phase composition. From the gas phase composition the composition of the adsorbed phase can be calculated. The results of the measurements are depicted in Figure 7 for all three materials. Each measurement features three graphs. The orange diamonds represent the total adsorption ( $n(C_2H_6)+n(C_2H_4)$ ) determined volumetrically. The blue circles and green triangles represent the adsorbed amount of  $C_2H_6$  and  $C_2H_4$  determined through gas chromatography, respectively. Between each point the sample was freshly activated. On each graph the first, second, third, etc. points are corresponding to each other and are derived from one measurement. Notably, the total amount adsorbed in all cases is always close to the respective adsorbed amounts in the high pressure adsorption isotherms shown in Figure 5. When **DMOF** is dosed with a binary mixture of ethane and ethylene at a total pressure of 157 kPa a total uptake of 1.90 mmol  $g^{-1}$  is recorded containing 1.12 mmol  $g^{-1}$  of  $C_2H_6$  and 0.78 mmol  $g^{-1}$  of  $C_2H_4$ . By increasing the pressure, an increase in total uptake and for both components is observed. At the highest measured total pressure of 1685 kPa a total uptake of 3.49 mmol  $g^{-1}$  is observed composed of 2.10 mmol  $g^{-1}$  ethane and 1.39 mmol  $g^{-1}$  ethylene. In the case of **DMOF-DM** a similar trend is observed (Figure 7b). The lowest pressure measured amounts to 129 kPa featuring a total uptake of 3.08 mmol  $g^{-1}$ . The uptakes of the individual components are 1.84 mmol  $g^{-1}$  and 1.24 mmol  $g^{-1}$  for ethane and ethylene

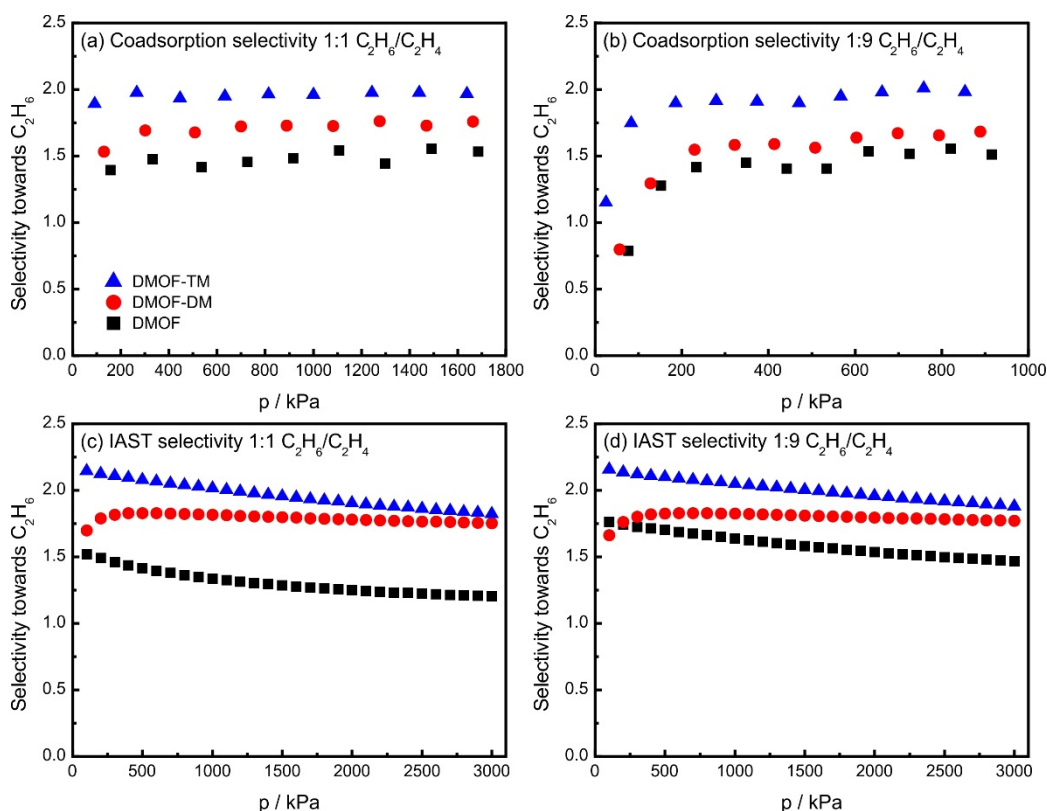


**Figure 8:** Adsorption selectivities for **DMOF** (black squares), **DMOF-DM** (red circles) and **DMOF-TM** (blue triangles) at 298 K for 1:1 (a, c) and 1:9 (b, d)  $C_2H_6/C_2H_4$  mixtures. Selectivities were determined through coadsorption (a, b) and derived from IAST calculations (c, d) using single component isotherms measured at 298 K.

respectively. Here also an increase of all components over the whole pressure range is observed reaching 4.40, 2.78 and 1.62  $mmol\ g^{-1}$  for the total, ethane and ethylene uptake, respectively at 1664 kPa. **DMOF-TM** shows the highest uptakes among the three materials (Figure 7c). At a pressure of 91 kPa the material reaches already higher uptakes than the other materials at the highest applied pressures. The total uptake amounts to 5.18  $mmol\ g^{-1}$  containing 2.98  $mmol\ g^{-1}$  and 2.20  $mmol\ g^{-1}$  of ethane and ethylene, respectively. In contrast to the other material not all components uptakes are increasing with increased pressure. In fact the ethylene uptake is decreasing from 2.20  $mmol\ g^{-1}$  to 2.01  $mmol\ g^{-1}$ , while the total uptake increased to 5.80  $mmol\ g^{-1}$  and the ethane uptake reaches 3.79  $mmol\ g^{-1}$  at a total pressure of 1637 kPa. For the experiments using a 10:90 ethane:ethylene mixture also preferential  $C_2H_6$  adsorption is observed. In the case of **DMOF** the lowest applied pressure is 77.06 kPa featuring a total uptake of 0.97  $mmol\ g^{-1}$ . The adsorbed  $C_2H_6$  and  $C_2H_4$  fractions amount to 0.09 and 0.89  $mmol\ g^{-1}$ . At the highest applied pressure (916 kPa) the uptake is 3.19  $mmol\ g^{-1}$  consisting of 2.74  $mmol\ g^{-1}$  ethylene and 0.45  $mmol\ g^{-1}$  ethane. For **DMOF-DM** a similar trend is observed. At 57 kPa the values are 1.93, 1.74 and 0.18  $mmol\ g^{-1}$  for total,  $C_2H_4$  and  $C_2H_6$  uptake, respectively. At the highest pressure point (889 kPa) the total recorded amount is 4.21  $mmol\ g^{-1}$ , consisting of 0.64  $mmol\ g^{-1}$  ethane and 3.57  $mmol\ g^{-1}$  ethylene. Finally, for **DMOF-TM** the highest uptakes are recorded. The lowest pressure measurement was conducted at 25 kPa featuring already a total uptake of 3.22  $mmol\ g^{-1}$ , consisting of 2.87  $mmol\ g^{-1}$  ethylene

and 0.36  $mmol\ g^{-1}$  ethane. At the highest applied pressure (854 kPa) the adsorbed amounts are further increasing to 5.78, 4.81 and 0.97  $mmol\ g^{-1}$  for the total, ethylene and ethane uptakes, respectively. Calculating the ratios of the adsorbates nicely illustrates the ethane scavenging ability of the materials. In the case of **DMOF-TM** the material is offered a 1:9 ethane:ethylene mixture at a total pressure of 853 kPa and the ratio of the adsorbates at equilibration is 1:4.5. Interestingly, at low pressures this ratio only amounts to 1:8, suggesting an improvement in sorption selectivity with an increase in pressure.

The co-adsorption measurements provide the concentrations of both components in the gas phase and in the adsorbate phase. By dividing the ratios of the components adsorbed through the ratio of the components in the gas phase the adsorption selectivity can be calculated. Figure 8 shows the calculated adsorption selectivities derived from the coadsorption measurements for  $C_2H_6:C_2H_4$  ratios of 1:1 (a) and 1:9 (b) (for tabulated values of  $q_n$  and  $p_n$  see ESI table S3 – S8). The lowest selectivities are observed for the pristine **DMOF**, which are in the range between 1.39 (157 kPa) and 1.55 (1492 kPa). This is well in line with the low pressure adsorption selectivity of the previously tested analogous material  $Ni_2(bdc)_2(dabco)$ .<sup>87</sup> Slightly higher selectivities were obtained for **DMOF-DM**, with  $S_{ads} = 1.57$  and 1.76 at 129 kPa and 1275 kPa, respectively. For **DMOF-TM** the selectivity is nearly pressure independent for 1:1 mixtures and stays close to  $S_{ads} = 1.9$ . The lowest observed value amounts to 1.89 kPa (91 kPa)

and the highest obtained value is 1.97 (267 kPa). These values are in the same range as for other high performance bulk ethane separation MOFs such as MUF-15<sup>37</sup> or PCN-250<sup>88</sup> and also comparable to Zn-atz-ipa ( $S_{IAST} = 2$ ) which was used as the ethane selective component in a sequential bed set up for C<sub>2</sub>H<sub>4</sub> separation from C<sub>2</sub>H<sub>2</sub>/C<sub>2</sub>H<sub>4</sub>/C<sub>2</sub>H<sub>6</sub>/CO<sub>2</sub> mixtures.<sup>89</sup> All MOFs that show higher ethane selectivities (i.e. Fe<sub>2</sub>(O<sub>2</sub>)dobdc<sub>2</sub>, Cu(Qc)<sub>2</sub>, MAF-49)<sup>35, 75, 90</sup> have considerably lower ethane uptake. In the case of a 1:9 mixture again a trend occurs that increasing the amount of methyl groups pointing into the pore space leads to a preferential adsorption of C<sub>2</sub>H<sub>6</sub>. In the case of **DMOF** and **DMOF-DM** even a slight preference towards ethylene is recorded at the lowest pressure points with C<sub>2</sub>H<sub>6</sub>/C<sub>2</sub>H<sub>4</sub> selectivities of 0.79 (at 77 kPa) and 0.80 (57 kPa), respectively. In the case of **DMOF-TM** ethane is favourably adsorbed at the lowest pressure point, with an adsorption selectivity of  $S_{ads} = 1.15$  (25 kPa). By increasing the pressures, a marked increase in ethane adsorption selectivities is observed reaching  $S_{ads}$  values of 1.54 (631 kPa), 1.67 (698 kPa) and 2.01 (758 kPa) for **DMOF**, **DMOF-DM** and **DMOF-TM**, respectively. The very low selectivities at low pressures can be in part attributed to the intrinsic measurement error of the instrument. Notably, Ma *et al.* also obtained low adsorption selectivities via IAST at low pressures for the Ni analogues using 1:15 C<sub>2</sub>H<sub>6</sub>:C<sub>2</sub>H<sub>4</sub> mixtures in their calculations.<sup>70</sup> The selectivity values also considerably increased with an increase in the overall pressure.

For comparison with the selectivities from coadsorption we also determined IAST selectivities in the range from 0-3000 kPa at 298 K for 1:1 and 1:9 ethane/ethylene mixtures (Figure 8c and d). Interestingly, the general trend in the coadsorption experiments suggests that the selectivity increases with an increase in pressure, however from the IAST studies a decrease in selectivity is observed for **DMOF** and **DMOF-TM** with an increase in pressure. For the material **DMOF-DM** in the range from 100-500 kPa an increase in selectivity is observed and then following in the range from 500-3000 kPa a slight decrease in selectivity is observed. For binary mixtures the IAST selectivities amount to 1.48 at 200 kPa and 1.27 at 1700 kPa, compared to values of 1.39 and 1.53 at these pressures derived from coadsorption. Hence, at 1700 kPa a 17 % difference between the selectivities derived through different methods is observed. When the pressure is further increased to 3000 kPa, IAST yields a low selectivity of only 1.2 for **DMOF**. For **DMOF-DM** these differences are not so pronounced. At low pressures (~100 kPa) the IAST selectivity amounts to 1.69, while the selectivity determined through coadsorption only amounts to 1.53. At higher pressures (~1700 kPa), the values are coinciding very well, amounting to 1.79 (IAST) and 1.76 (coadsorption). At 3000 kPa the IAST selectivity is 1.75. For **DMOF-TM** the low pressure selectivity determined from IAST at 100 kPa is 2.14 while the coadsorption at this pressure only amounts to 1.89, which is a 12 % difference. Finally, at high pressures the IAST and coadsorption are very similar, amounting to 1.93 and 1.96, respectively, at 1700 kPa. The IAST values determined from the low pressure and high pressure sets of isotherms are very similar for the materials, except for the case of **DMOF-TM**, where the IAST at 100 kPa is determined as 2.14 (high pressure

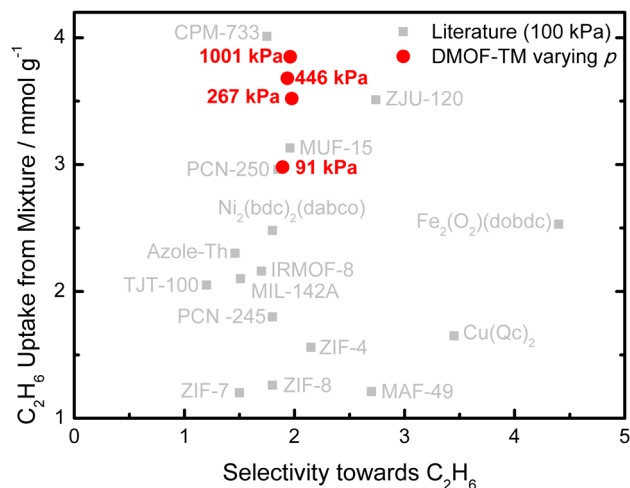


**Figure 9:** Comparison of the ethane uptake vs C<sub>2</sub>H<sub>6</sub>/C<sub>2</sub>H<sub>4</sub> adsorption selectivity for high performance MOFs. Grey squares symbolize values from the literature derived from IAST theory for equimolar binary mixtures at 100 kPa. Red circles represent values for **DMOF-TM** obtained through coadsorption measurements at different pressures.

isotherms) and 1.88 (low pressure isotherms). For the 1:9 mixtures generally the IAST values are always higher than the values obtained through coadsorption. Particularly at low pressures, the IAST and coadsorption selectivities do not match well at all. For instance, at ~100 kPa, **DMOF** has an IAST selectivity of 1.76, while the value from coadsorption amounts to only 0.79. A similar observation was made for **DMOF-DM**, where the selectivity from coadsorption amounted to 0.80 and the IAST selectivity is more than double with 1.66. For **DMOF-TM**, this discrepancy is not as severe, with a IAST selectivity of 2.16 and a coadsorption selectivity of 1.74 at 100 kPa, which is a difference of 19 %. At higher pressures (~900 kPa) the IAST selectivities and the selectivities derived from coadsorption are more similar to each other. In the case of **DMOF** these values are 1.65 (IAST) and 1.51 (coadsorption), for **DMOF-DM** 1.82 (IAST) and 1.68 (coadsorption) and for **DMOF-TM** 2.05 (IAST) and 1.98 (coadsorption).

#### Comparison with the Literature

To set this work into context, we compared the results with pertinent examples from the literature (Figure 9).<sup>35, 37-39, 70, 75, 87-88, 90-99</sup> A table with key properties of ethane selective MOFs can be found in supporting information (ESI Table S9). In general, a balancing act between uptake and selectivity needs to be overcome. High selectivity materials tend to have lower uptakes, for instance the top performers MAF-49 and Cu(Qc)<sub>2</sub> have among the highest reported ethane selectivities for 1:1 mixtures at 100 kPa amounting to 2.7 and 3.45, however their ethane uptakes from the mixture are considerably low with 1.21 and 1.65 mmol g<sup>-1</sup> which might hamper the ethylene production. Materials that show similar selectivities and ethane uptakes to our material are MUF-15 and PCN-250, which have selectivities of 1.96 and 1.85 and feature ethane uptakes of 3.13 and 2.96 mmol g<sup>-1</sup>. The selectivities of **DMOF-TM** amount to 1.89 for a 50:50 mixture of ethane and ethylene while taking up 2.98 mmol g<sup>-1</sup> of ethane at 91 kPa and increase to 1.96 at 1001 kPa with an ethane uptake of 3.85 mmol g<sup>-1</sup>. The steady increase

of uptake without losing selectivity with increased pressure, suggests the potential for driving separations at higher operating pressures with the probability of an increased throughput. Another metric that is sometimes discussed in the literature is the separation potential  $\Delta Q$  which sets the capacity and the selectivity into relation.<sup>100</sup> The top performing materials here are  $\text{Fe}_2(\text{O}_2)\text{dobdc}$  and CPM-733<sup>97</sup> with values of 1.93 and 1.88 at a pressure of 1 bar for an equimolar mixture. Interestingly **DMOF-TM** shows only a low separation potential of 0.78 at 91.14 kPa, however this dramatically increases to 1.95 at high pressures (1637 kPa) making this material compatible with other top performers. Particularly, considering that the ethane adsorption isotherms do not reach saturation uptake at 100 kPa which is used in many studies for benchmarking, a lot of materials' performance might be boosted through movement to a different pressure regime, which is anyhow more amenable for industrial applications.<sup>101</sup>

## Conclusion

In this contribution we present a series of three pillared-layered MOFs based on  $\text{Zn}_2$  paddle-wheels, dabco pillars and three different benzenedicarboxylate based linker molecules which only differ in the amount of  $-\text{CH}_3$  groups attached to the benzene core. Adsorption isotherms of the materials show a preferential uptake of ethane over ethylene. Whereas the slope of the adsorption isotherms is getting steeper with an increase in methylation, most likely through the better confinement of the guest molecules in the pore space. Calculation of  $Q_{st}$  via the Clausius-Clapeyron equation also provide higher isosteric heats of adsorption for the tetramethyl functionalized material, **DMOF-TM**. Molecular Simulations were used to identify favourable adsorption sites and were able to highlight the benefit of the methyl groups which form a pocket that strongly adsorbs ethane molecules. High pressure adsorption measurements until pressures of 3000 kPa were conducted to see how higher pressures affect the adsorption properties and selectivities. Interestingly it can be concluded that by increasing the adsorption pressure the selectivity increases until reaching a plateau which is kept in all cases over the whole pressure range. Notably, the ethane uptake is increasing over the whole pressure range. This suggests that the materials can maintain at higher pressures the selectivity while improving the throughput of a reactor bed. We believe that it is crucial to look at adsorption selectivities beyond 100 kPa also in the case of adsorptive hydrocarbon separation to identify the usable parameter space for engineers when developing real-life application of research-sorbents using pressure swing adsorption with a good working capacity. Further, the implementation of methyl groups might also be a viable design element for the construction of dual function MOFs which can separate ethane and acetylene simultaneously from ethylene streams.

## Author Contributions

A.S., N.C.B and S.N. conceptualized the project. A.S. synthesized and characterized the studied materials. T.T., J.Y. K.S. and S.N. conducted gas adsorption and breakthrough experiments. J.D.E. provided DFT simulations of adsorption sites. A.S. and Y.H. processed and analysed adsorption data. Y.K. conducted SEM measurements. A.S., T.T., N.C.B. and S.N. wrote the manuscript with contributions from all co-authors.

## Conflicts of interest

There are no conflicts to declare.

## Acknowledgements

A.S. gratefully acknowledges the German Research Foundation (DFG) for a postdoctoral fellowship (SCHN 1539/1-1). This work was supported in part by the Cooperative Research Program of Institute for Catalysis, Hokkaido University (20B1030). J.D.E. acknowledges the support of the Alexander von Humboldt foundation and HPC platforms provided by the Center for Information Services and High Performance Computing (ZIH) at TU Dresden. This work was partially supported by JSPS KAKENHI (JPH04570 to Y.H.) N.C.B. acknowledges support from the Sandia National Laboratories Truman Fellowship Program, which is funded by the Laboratory Directed Research and Development (LDRD) Program. Sandia National Laboratories is a multi-mission laboratory managed and operated by National Technology and Engineering Solutions of Sandia, LLC., a wholly owned subsidiary of Honeywell International, Inc., for the U.S. Department of Energy's National Nuclear Security Administration under contract DE-NA0003525. This paper describes objective technical results and analysis. Any subjective views or opinions that might be expressed in the paper do not necessarily represent the views of the U.S. Department of Energy or the United States Government.

## Notes and references

- 1 A. B. d. Haan and H. Bosch, *Industrial Separation Processes: Fundamentals*, De Gruyter, 2013.
- 2 D. S. Sholl and R. P. Lively, *Nature*, 2016, **532**, 435-437.
- 3 R. B. Eldrige, *Ind. Eng. Chem. Res.*, 1993, **32**, 2208-2212.
- 4 Y. Wang, S. B. Peh and D. Zhao, *Small*, 2019, **15**, 1900058.
- 5 L. Yang, S. Qian, X. Wang, X. Cui, B. Chen and H. Xing, *Chem. Soc. Rev.*, 2020, **49**, 5359-5406.
- 6 K. Adil, Y. Belmabkhout, R. S. Pillai, A. Cadiau, P. M. Bhatt, A. H. Assen, G. Maurin and M. Eddaoudi, *Chem. Soc. Rev.*, 2017, **46**, 3402-3430.
- 7 B. R. Barnett, M. I. Gonzalez and J. R. Long, *Trends Chem.*, 2019, **1**, 159-171.
- 8 S. Mukherjee, D. Sensharma, K.-J. Chen and M. J. Zaworotko, *Chem. Commun.*, 2020, **56**, 10419-10441.
- 9 C. S. Diercks, M. J. Kalmutzki, N. J. Diercks and O. M. Yaghi, *ACS Cent. Sci.*, 2018, **4**, 1457-1464.
- 10 Z. Ji, H. Wang, S. Canossa, S. Wuttke and O. M. Yaghi, *Adv. Funct. Mater.*, 2020, **30**, 2000238.
- 11 H. Lyu, Z. Ji, S. Wuttke and O. M. Yaghi, *Chem*, 2020, **6**, 2219-2241.

- 12 W. Xu, B. Tu, Q. Liu, Y. Shu, C.-C. Liang, C. S. Diercks, O. M. Yaghi, Y.-B. Zhang, H. Deng and Q. Li, *Nat. Rev. Mater.*, 2020, **5**, 764-779.
- 13 L. Feng, K.-Y. Wang, G. S. Day and H.-C. Zhou, *Chem. Soc. Rev.*, 2019, **48**, 4823-4853.
- 14 L. Feng, G. S. Day, K.-Y. Wang, S. Yuan and H.-C. Zhou, *Chem*, 2020, **6**, 2902-2923.
- 15 L. Feng, J. Pang, P. She, J.-L. Li, J.-S. Qin, D.-Y. Du and H.-C. Zhou, *Adv. Mater.*, 2020, **32**, 2004414.
- 16 L. Feng, K.-Y. Wang, J. Willman and H.-C. Zhou, *ACS Cent. Sci.*, 2020, **6**, 359-367.
- 17 I. Senkovska and S. Kaskel, *Chem. Commun.*, 2014, **50**, 7089-7098.
- 18 Z. Bao, J. Wang, Z. Zhang, H. Xing, Q. Yang, Y. Yang, H. Wu, R. Krishna, W. Zhou, B. Chen and Q. Ren, *Angew. Chem., Int. Ed.*, 2018, **57**, 16020-16025.
- 19 R.-B. Lin, L. Li, H.-L. Zhou, H. Wu, C. He, S. Li, R. Krishna, J. Li, W. Zhou and B. Chen, *Nat. Mater.*, 2018, **17**, 1128-1133.
- 20 A. Cadiou, K. Adil, P. M. Bhatt, Y. Belmabkhout and M. Eddaoudi, *Science*, 2016, **353**, 137-140.
- 21 B. Liang, X. Zhang, Y. Xie, R.-B. Lin, R. Krishna, H. Cui, Z. Li, Y. Shi, H. Wu, W. Zhou and B. Chen, *J. Am. Chem. Soc.*, 2020, **142**, 17795-17801.
- 22 T. Liu, H. Cui, X. Zhang, Z.-Y. Zhang, R.-B. Lin, B. Liang, J. Zhang, D. Li and B. Chen, *ACS Appl. Mater. Interfaces*, 2020, **12**, 48712-48717.
- 23 J. Wang, Y. Zhang, P. Zhang, J. Hu, R.-B. Lin, Q. Deng, Z. Zeng, H. Xing, S. Deng and B. Chen, *J. Am. Chem. Soc.*, 2020, **142**, 9744-9751.
- 24 S. Mukherjee, N. Kumar, A. A. Bezrukov, K. Tan, T. Pham, K. A. Forrest, K. Oyekan, O. T. Qazvini, D. G. Madden, B. Space and M. Zaworotko, *Angew. Chem., Int. Ed.*, 2021, **60**, 10902-10909.
- 25 A. Schneemann, E. D. Bloch, S. Henke, P. L. Llewellyn, J. R. Long and R. A. Fischer, *Chem. - Eur. J.*, 2015, **21**, 18764-18769.
- 26 A. Schneemann, Y. Takahashi, R. Rudolf, S.-i. Noro and R. A. Fischer, *J. Mater. Chem. A*, 2016, **4**, 12963-12972.
- 27 O. T. Qazvini, R. Babarao and S. G. Telfer, *Chem. Mater.*, 2019, **31**, 4919-4926.
- 28 E. D. Bloch, W. L. Queen, R. Krishna, J. M. Zadrozny, C. M. Brown and J. R. Long, *Science*, 2012, **335**, 1606-1610.
- 29 S. J. Geier, J. A. Mason, E. D. Bloch, W. L. Queen, M. R. Hudson, C. M. Brown and J. R. Long, *Chemical Science*, 2013, **4**, 2054-2061.
- 30 G. R. Loring, B. A. Trump, C. M. Brown and E. D. Bloch, *Chem. Mater.*, 2017, **29**, 8583-8587.
- 31 J. E. Bachman, M. T. Kapelewski, D. A. Reed, M. I. Gonzalez and J. R. Long, *J. Am. Chem. Soc.*, 2017, **139**, 15363-15370.
- 32 D. M. Ruthven and S. C. Reyes, *Microporous Mesoporous Mater.*, 2007, **104**, 59-66.
- 33 C. M. Shu, S. Kulvaranon, M. E. Findley and A. I. Liapis, *Sep. Technol.*, 1990, **1**, 18-28.
- 34 D. L. Peterson, F. G. Helfferich and R. K. Griep, 1968.
- 35 R.-B. Lin, H. Wu, L. Li, X.-L. Tang, Z. Li, J. Gao, H. Cui, W. Zhou and B. Chen, *J. Am. Chem. Soc.*, 2018, **140**, 12940-12946.
- 36 J. Pires, M. L. Pinto and V. K. Saini, *ACS Appl. Mater. Interfaces*, 2014, **6**, 12093-12099.
- 37 O. T. Qazvini, R. Babarao, Z.-L. Shi, Y.-B. Zhang and S. G. Telfer, *J. Am. Chem. Soc.*, 2019, **141**, 5014-5020.
- 38 Z. Xu, X. Xiong, J. Xiong, R. Krishna, L. Li, Y. Fan, F. Luo and B. Chen, *Nat. Commun.*, 2020, **11**, 3163.
- 39 J. Pei, J.-X. Wang, K. Shao, Y. Yang, Y. Cui, H. Wu, W. Zhou, B. Li and G. Qian, *J. Mater. Chem. A*, 2020, **8**, 3613-3620.
- 40 D. Lv, J. Chen, Y. Chen, Z. Liu, Y. Xu, C. Duan, H. Wu, Y. Wu, J. Xiao, H. Xi, Z. Li and Q. Xia, *AIChE J.*, 2019, **65**, e16616.
- 41 A. Dinh, H. Yang, F. Peng, T. C. Nguyen, A. Hong, P. Feng and X. Bu, *Cryst. Growth Des.*, 2020, **20**, 3523-3530.
- 42 H. Xiang, Y. Shao, A. Ameen, H. Chen, W. Yang, P. Gorgojo, F. R. Siperstein, X. Fan and Q. Pan, *Sep. Purif. Technol.*, 2020, **242**, 116819.
- 43 M. C. Kroon and L. F. Vega, *Langmuir*, 2009, **25**, 2148-2152.
- 44 K. Maeda, J. Akimoto, Y. Kiyozumi and F. Mizukami, *Angew. Chem., Int. Ed.*, 1995, **34**, 1199-1201.
- 45 V. Bon, J. Pallmann, E. Eisbein, H. C. Hoffmann, I. Senkovska, I. Schwedler, A. Schneemann, S. Henke, D. Wallacher, R. A. Fischer, G. Seifert, E. Brunner and S. Kaskel, *Microporous Mesoporous Mat.*, 2015, **216**, 64-74.
- 46 N. C. Burtch, D. Dubbeldam and K. S. Walton, *Mol. Simul.*, 2015, **41**, 1379-1387.
- 47 N. C. Burtch and K. S. Walton, *Acc. Chem. Res.*, 2015, **48**, 2850-2857.
- 48 H. Jasuja, N. C. Burtch, Y.-g. Huang, Y. Cai and K. S. Walton, *Langmuir*, 2013, **29**, 633-642.
- 49 N. C. Burtch, A. Torres-Knoop, G. S. Foo, J. Leisen, C. Sievers, B. Ensing, D. Dubbeldam and K. S. Walton, *J. Phys. Chem. Lett.*, 2015, **6**, 812-816.
- 50 S. Xing, J. Liang, P. Brandt, F. Schäfer, A. Nuhnen, T. Heinen, I. Boldog, J. Möllmer, M. Lange, O. Weingart and C. Janiak, *Angew. Chem., Int. Ed.*, 2021, **n/a**.
- 51 S. J. Baxter, A. Schneemann, A. D. Ready, P. Wijeratne, A. P. Wilkinson and N. C. Burtch, *J. Am. Chem. Soc.*, 2019, **141**, 12849-12854.
- 52 N. C. Burtch, S. J. Baxter, J. Heinen, A. Bird, A. Schneemann, D. Dubbeldam and A. P. Wilkinson, *Adv. Funct. Mater.*, 2019, **29**, 1904669.
- 53 J. Pires, J. Fernandes, K. Dedecker, J. R. B. Gomes, G. Pérez-Sánchez, F. Nouar, C. Serre and M. L. Pinto, *ACS Appl. Mater. Interfaces*, 2019, **11**, 27410-27421.
- 54 X. Cai, F. Gharagheizi, L. W. Bingel, D. Shade, K. S. Walton and D. S. Sholl, *Ind. Eng. Chem. Res.*, 2021, **60**, 639-651.
- 55 A. Nuhnen and C. Janiak, *Dalton Trans.*, 2020, **49**, 10295-10307.
- 56 A. L. Myers and J. M. Prausnitz, *AIChE J.*, 1965, **11**, 121-127.
- 57 P. Iacomini and P. L. Llewellyn, *Chem. Mater.*, 2020, **32**, 982-991.
- 58 J. D. Evans, V. Bon, I. Senkovska and S. Kaskel, *Langmuir*, 2021, **37**, 4222-4226.
- 59 S. Spicher and S. Grimme, *Angew. Chem., Int. Ed.*, 2020, **59**, 15665-15673.
- 60 C. Bannwarth, S. Ehlert and S. Grimme, *J. Chem. Theory Comput.*, 2019, **15**, 1652-1671.
- 61 P. Pracht, F. Bohle and S. Grimme, *Phys. Chem. Chem. Phys.*, 2020, **22**, 7169-7192.
- 62 D. N. Dybtsev, H. Chun and K. Kim, *Angew. Chem., Int. Ed.*, 2004, **43**, 5033-5036.
- 63 H. Chun, D. N. Dybtsev, H. Kim and K. Kim, *Chem. Eur. J.*, 2005, **11**, 3521-3529.
- 64 H. Uehara, S. Diring, S. Furukawa, Z. Kalay, M. Tsotsalas, M. Nakahama, K. Hirai, M. Kondo, O. Sakata and S. Kitagawa, *J. Am. Chem. Soc.*, 2011, **133**, 11932-11935.
- 65 R. Lyndon, W. You, Y. Ma, J. Bacsa, Y. Gong, E. E. Stangland, K. S. Walton, D. S. Sholl and R. P. Lively, *Chem. Mater.*, 2020, **32**, 3715-3722.
- 66 C. Y. Lee, Y.-S. Bae, N. C. Jeong, O. K. Farha, A. A. Sarjeant, C. L. Stern, P. Nickias, R. Q. Snurr, J. T. Hupp and S. T. Nguyen, *J. Am. Chem. Soc.*, 2011, **133**, 5228-5231.

- 67 H. Miura, V. Bon, I. Senkovska, S. Ehrling, S. Watanabe, M. Ohba and S. Kaskel, *Dalton Trans.*, 2017, **46**, 14002-14011.
- 68 S. Wannapaiboon, A. Schneemann, I. Hante, M. Tu, K. Epp, A. L. Semrau, C. Sternemann, M. Paulus, S. J. Baxter, G. Kieslich and R. A. Fischer, *Nat. Commun.*, 2019, **10**, 346.
- 69 L. Abylgazina, I. Senkovska, R. Engemann, S. Ehrling, T. E. Gorelik, N. Kavoosi, U. Kaiser and S. Kaskel, *Front. Chem.*, 2021, **9**, 674566.
- 70 X. Wang, Z. Niu, A. M. Al-Enizi, A. Nafady, Y. Wu, B. Aguila, G. Verma, L. Wojtas, Y.-S. Chen, Z. Li and S. Ma, *J. Mater. Chem. A*, 2019, **7**, 13585-13590.
- 71 K. Uemura, Y. Yamasaki, Y. Komagawa, K. Tanaka and H. Kita, *Angew. Chem., Int. Ed.*, 2007, **46**, 6662-6665.
- 72 L. Abylgazina, I. Senkovska, S. Ehrling, V. Bon, P. St. Petkov, J. D. Evans, S. Krylova, A. Krylov and S. Kaskel, *CrystEngComm*, 2021, **23**, 538-549.
- 73 S. Henke, A. Schneemann, A. Wütscher and R. A. Fischer, *J. Am. Chem. Soc.*, 2012, **134**, 9464-9474.
- 74 Z. Wang and S. M. Cohen, *J. Am. Chem. Soc.*, 2009, **131**, 16675-16677.
- 75 L. Li, R.-B. Lin, R. Krishna, H. Li, S. Xiang, H. Wu, J. Li, W. Zhou and B. Chen, *Science*, 2018, **362**, 443-446.
- 76 M. Wriedt, J. P. Sculley, A. A. Yakovenko, Y. Ma, G. J. Halder, P. B. Balbuena and H.-C. Zhou, *Angew. Chem., Int. Ed.*, 2012, **51**, 9804-9808.
- 77 J. Smukala, R. Span and W. Wagner, *J. Phys. Chem. Ref. Data*, 2000, **29**, 1053-1121.
- 78 D. G. Friend, H. Ingham and J. F. Fly, *J. Phys. Chem. Ref. Data*, 1991, **20**, 275-347.
- 79 F.-X. Coudert, *Phys. Chem. Chem. Phys.*, 2010, **12**, 10904-10913.
- 80 F.-X. Coudert, C. Mellot-Draznieks, A. H. Fuchs and A. Boutin, *J. Am. Chem. Soc.*, 2009, **131**, 11329-11331.
- 81 L. Hamon, P. L. Llewellyn, T. Devic, A. Ghoufi, G. Clet, V. Guillermin, G. D. Pirngruber, G. Maurin, C. Serre, G. Driver, W. van Beek, E. Jolimaître, A. Vimont, M. Daturi and G. Férey, *J. Am. Chem. Soc.*, 2009, **131**, 17490-17499.
- 82 J. Heinen, N. C. Burtch, K. S. Walton, C. Fonseca Guerra and D. Dubbeldam, *Chem. Eur. J.*, 2016, **22**, 18045-18050.
- 83 J. Möllmer, M. Lange, A. Möller, C. Patzschke, K. Stein, D. Lässig, J. Lincke, R. Gläser, H. Krautscheid and R. Staudt, *Journal of Materials Chemistry*, 2012, **22**, 10274-10286.
- 84 A. U. Ortiz, M.-A. Springuel-Huet, F.-X. Coudert, A. H. Fuchs and A. Boutin, *Langmuir*, 2012, **28**, 494-498.
- 85 K. Tan, S. Zuluaga, Q. Gong, Y. Gao, N. Nijem, J. Li, T. Thonhauser and Y. J. Chabal, *Chem. Mater.*, 2015, **27**, 2203-2217.
- 86 P. Vervoorts, A. Schneemann, I. Hante, J. Pirillo, Y. Hijikata, T. Toyao, K. Kon, K.-i. Shimizu, T. Nakamura, S.-i. Noro and R. A. Fischer, *ACS Appl. Mater. Interfaces*, 2020, **12**, 9448-9456.
- 87 W. Liang, F. Xu, X. Zhou, J. Xiao, Q. Xia, Y. Li and Z. Li, *Chem. Eng. Sci.*, 2016, **148**, 275-281.
- 88 Y. Chen, Z. Qiao, H. Wu, D. Lv, R. Shi, Q. Xia, J. Zhou and Z. Li, *Chem. Eng. Sci.*, 2018, **175**, 110-117.
- 89 K.-J. Chen, D. G. Madden, S. Mukherjee, T. Pham, K. A. Forrest, A. Kumar, B. Space, J. Kong, Q.-Y. Zhang and M. J. Zaworotko, *Science*, 2019, **366**, 241-246.
- 90 P.-Q. Liao, W.-X. Zhang, J.-P. Zhang and X.-M. Chen, *Nat. Commun.*, 2015, **6**, 8697.
- 91 Y. Chen, H. Wu, D. Lv, R. Shi, Y. Chen, Q. Xia and Z. Li, *Ind. Eng. Chem. Res.*, 2018, **57**, 4063-4069.
- 92 D. Lv, R. Shi, Y. Chen, Y. Wu, H. Wu, H. Xi, Q. Xia and Z. Li, *ACS Appl. Mater. Interfaces*, 2018, **10**, 8366-8373.
- 93 C. Gücüyener, J. van den Bergh, J. Gascon and F. Kapteijn, *J. Am. Chem. Soc.*, 2010, **132**, 17704-17706.
- 94 U. Böhme, B. Barth, C. Paula, A. Kuhnt, W. Schwieger, A. Mundstock, J. Caro and M. Hartmann, *Langmuir*, 2013, **29**, 8592-8600.
- 95 M. Hartmann, U. Böhme, M. Hovestadt and C. Paula, *Langmuir*, 2015, **31**, 12382-12389.
- 96 C.-X. Chen, Z.-W. Wei, T. Pham, P. C. Lan, L. Zhang, K. A. Forrest, S. Chen, A. M. Al-Enizi, A. Nafady, C.-Y. Su and S. Ma, *Angew. Chem., Int. Ed.*, 2021, **60**, 9680-9685.
- 97 H. Yang, Y. Wang, R. Krishna, X. Jia, Y. Wang, A. N. Hong, C. Dang, H. E. Castillo, X. Bu and P. Feng, *J. Am. Chem. Soc.*, 2020, **142**, 2222-2227.
- 98 B. Zhu, J.-W. Cao, S. Mukherjee, T. Pham, T. Zhang, T. Wang, X. Jiang, K. A. Forrest, M. J. Zaworotko and K.-J. Chen, *J. Am. Chem. Soc.*, 2021, **143**, 1485-1492.
- 99 H.-G. Hao, Y.-F. Zhao, D.-M. Chen, J.-M. Yu, K. Tan, S. Ma, Y. Chabal, Z.-M. Zhang, J.-M. Dou, Z.-H. Xiao, G. Day, H.-C. Zhou and T.-B. Lu, *Angew. Chem., Int. Ed.*, 2018, **57**, 16067-16071.
- 100 R. Krishna, *RSC Adv.*, 2017, **7**, 35724-35737.
- 101 R. T. Yang, *Gas separation by adsorption processes*, Imperial College Press, London, 1997.
- 102